ELSEVIER

International Journal of Solids and Structures 41 (2004) 5697–5716

INTERNATIONAL JOURNAL OF SOLIDS and STRUCTURES

www.elsevier.com/locate/ijsolstr

Dynamic spherical cavity expansion in a pressure sensitive elastoplastic medium

David Durban, Rami Masri *,[1]

Faculty of Aerospace Engineering, Technion, Haifa 32000, Israel

Received 29 July 2003; received in revised form 14 March 2004
Available online 1 June 2004

Abstract

The self-similar elastoplastic field induced by dynamic expansion of a pressurized spherical cavity is investigated for pressure sensitive solids. Material behavior is described by the hypoelastic model of the Drucker–Prager material with a non-associated flow rule, with arbitrary strain-hardening. We examine in detail the external elastic field, which is expected to develop at a distance from the cavity prior to plastic yielding. A new observation that emerges from that elastic solution is the possible existence of a compressive elastic zone where yielding is prevented since the effective stress remains negative. Simple analytical solutions are given for the fully incompressible elastic/perfectly plastic material with a non-associated flow rule. In particular, we study the influence of plastic pressure sensitivity on the dynamic cavitation pressure. A few useful relations are derived for the cavitation pressure which reveal the coupled effect of plastic pressure sensitivity and material inertia. A separate numerical analysis is given for the fully incompressible strain-hardening solid with a non-associated flow rule. Several numerical illustrations are presented for the solid with an associated flow rule along with a plastic boundary layer analysis for the thin singular zone near the cavity wall.

Keywords: Spherical cavity expansion; Dynamic cavitation; Penetration; Pressure sensitive plasticity; Dynamic material behavior; Dynamic plasticity

1. Introduction

The dynamic elastoplastic field induced by a pressurized spherical cavity expanding in an infinite medium is widely used in simulating penetration phenomena. The simplicity offered by the spherical symmetric pattern of the deforming material leads to fairly simple, yet accurate, expressions for key parameters like the resisting force and penetration depth. An extensive review of earlier work has been given by Hopkins (1960) with emphasis on incompressible Mises elastic/perfectly plastic models. Elastic

* Corresponding author. Tel.: +1-972-4-829-3805; fax: +1-972-4-829-2030.
E-mail address: masri@aerodyne.technion.ac.il (R. Masri).
[1] This work is based in part on a Master of Science thesis submitted to the Technion by Rami Masri.

0020-7683/$ - see front matter © 2004 Elsevier Ltd. All rights reserved.
doi:10.1016/j.ijsolstr.2004.03.009

Nomenclature

A	instantaneous radius of pressurized spherical cavity
$\dot{A}$	cavity expansion velocity (constant)
C	integration constant in the linear small strains elastic solution
C_{E}	linear elastic dilatation wave speed
$\mathbf{D}$	Eulerian strain rate tensor
E	elastic modulus
G	non-dimensionalized plastic potential
$\mathbf{I}$	second order unit tensor
K	material parameter in the Ramberg–Osgood power law
M	cavity expansion Mach number
P_{c}	non-dimensionalized cavitation pressure
R	radial coordinate of a spherical system
$\dot{R}$	radial material velocity
$\mathbf{S}$	stress deviator tensor
V	non-dimensionalized radial velocity
Y	yield stress
g	plastic potential
m	non-dimensionalized cavity expansion velocity
n	hardening index in the Ramberg–Osgood power law
p_{c}	cavitation pressure
v	radial material velocity
Σ	non-dimensionalized effective stress
Σ_{y}	non-dimensional yield stress
Σ_{r}, Σ_θ	non-dimensionalized stresses
β	elastic-compressibility parameter
δ	plastic boundary layer coordinate
ϵ	total strain
ϵ_{p}	effective plastic strain
$\dot{\epsilon}_{\mathrm{p}}$	effective plastic strain rate
$\dot{\epsilon}_{\mathrm{r}}$, $\dot{\epsilon}_\theta = \dot{\epsilon}_\phi$	Eulerian strain rate components in spherical-symmetric field
η, μ	parameters to reflect the plastic pressure sensitivity
ν	Poisson's ratio
ξ	non-dimensional radial coordinate
ξ_{i}	elastic/plastic interface
ξ_{w}	rigid/elastic wave front
ξ_0	inner radius where the effective stress vanishes
ρ	density of the deformed field
ρ_0	reference density of the undeformed stress free state
$\boldsymbol{\sigma}$	Cauchy stress tensor
$\check{\boldsymbol{\sigma}}$	Jaumann stress rate
σ_{e}	effective stress
σ_{h}	hydrostatic stress
σ_{r}, $\sigma_\theta = \sigma_\phi$	Cauchy stress components in spherical-symmetric field
τ	Mises effective stress

Superposed dot and superposed prime denote differentiation with respect to time and ξ respectively.

compressibility in dynamic spherical cavity expansion has been considered by Forrestal and Luk (1988) for an elastic/perfectly plastic Tresca solid along with a linear pressure–dilatation relation. A pure power law for strain-hardening, again for the Tresca material, is examined by Luk et al. (1991), for both compressible and incompressible elastic response.

In recent years, interest in the problem of penetration into concrete and geomaterial media has promoted a number of publications on dynamic cavity expansion in pressure sensitive solids. A Mohr–Coulomb type model in conjunction with elastic/perfectly plastic behavior has been employed by Forrestal and Tzou (1997) to investigate penetration into concrete targets. Earth penetration is studied by Macek and Duffey (2000) with Mohr–Coulomb plasticity that allows for damage. Dynamic spherical expansion in brittle ceramics is investigated by Satapathy (2001), again with a Mohr–Coulomb type constitutive behavior, assuming that there is no cohesion in the plastic range.

In the present paper, we attempt to present a unified treatment of dynamic spherical expansion in a pressure sensitive elastoplastic medium (Masri, 2001). Material response is modelled by the hypoelastic theory for the material with a non-associated Drucker–Prager solid (Durban and Fleck, 1997). The theory accounts for both elastic and plastic compressibility and allows for arbitrary strain-hardening in the plastic range.

In the next section, we begin with a brief exposition of the governing dynamic field equations following the quasi-static spherical cavity expansion analysis of Durban and Fleck (1997). Assuming a self-similar expansion field we show that the governing system consists of four ordinary differential equations with two stress components, radial velocity and density as unknowns.

Next, in Section 3, we examine the external elastic field, which is expected to develop at a distance from the cavity prior to plastic yielding. The governing system is reduced here to just two equations for the stresses, which can be further simplified, under the assumption of small elastic-stresses, to the standard linear elastic model. This gives the known elastic dilatation wave speed for the rigid/elastic interface, thus setting the outer limit for the process zone. However, a new observation that emerges from the elastic solution is the possible existence of a compressive elastic zone where yielding is prevented since the effective stress remains negative. A simple expression for the location of the inner boundary of that zone is derived along with a condition for its existence, which is due to plastic pressure sensitivity and Poisson's ratio.

The important case of a fully incompressible solid (where both elastic and plastic branches do not admit volume changes), which is also an extreme case of non-associativity, is discussed in some detail in Section 4. The velocity profile behaves here as the inverse square of radial distance with the deforming field extending to infinity. A quadrature type solution is given for the stresses with the elastic/perfectly plastic characteristic. The location of the elastic/plastic interface and the cavitation pressure are approximated by closed form expressions at different levels of accuracy. We have found that plastic pressure sensitivity causes an increase in the cavitation pressure but reduces the size of the plastic zone. These results are supported by a numerical solution for the stresses in a fully incompressible elastic/power-hardening material. In the absence of pressure sensitivity, we recover the closed form solution for the incompressible Mises material, which is valid for any hardening or softening characteristic.

Section 5 is devoted to the material with an associated Drucker–Prager flow rule and we show, with no further assumptions, that the exact field equations can be reduced to two equations for the stresses. A few numerical solutions for both compressible and incompressible response reveal the coupled effect of plastic pressure sensitivity and material inertia in raising the level of cavitation pressure. By comparison, plastic compressibility appears to be much more important than elastic compressibility at low expansion velocities.

The paper concludes with an asymptotic analysis of the near cavity plastic boundary layer, for solids with an associated flow rule. Plastic strain at the cavity's wall is unbounded but it decays with distance. It is shown that strain-hardening raises effective stress gradients within the boundary layer.

2. Steady self-similar dynamic expansion of a spherical cavity

Consider a pressurized spherical cavity (Fig. 1) of instantaneous radius A expanding under self-similar conditions in an infinite medium. The surrounding spherical-symmetric stress field has the active Cauchy components σ_r, $\sigma_\theta = \sigma_\phi$ with the radial equation of motion

$$\frac{d\sigma_r}{dR} + \frac{2}{R}(\sigma_r - \sigma_\theta) = \rho \dot{v}, \tag{1}$$

where R is the radial coordinate of a spherical system (R, θ, ϕ), with the origin at the center of the cavity, ρ is the density, $v = \dot{R}$ is the radial material velocity and a superposed dot denotes differentiation with respect to time. Now, in steady-state expansion we assume that the only independent variable is the non-dimensional radial coordinate $\xi = R/A$. Thus, the time derivative is transformed by the similarity relation (Durban and Fleck, 1997)

$$\dot{(\,)} = \dot{\xi}\frac{d(\,)}{d\xi} = \left(\frac{\dot{R}}{A} - \xi\frac{\dot{A}}{A}\right)\frac{d(\,)}{d\xi} = \frac{\dot{A}}{A}(V - \xi)\frac{d(\,)}{d\xi}, \tag{2}$$

with $V = \dot{R}/\dot{A}$ denoting the non-dimensional radial velocity; now, since $v = \dot{A}V$ we have for constant $\dot{A}$ that $\dot{v} = \dot{A}\dot{V}$, and it follows from (2) that (1) can be rewritten as

$$\Sigma_r' + \frac{2}{\xi}(\Sigma_r - \Sigma_\theta) = m^2\left(\frac{\rho}{\rho_0}\right)(V - \xi)V', \tag{3}$$

where $(\Sigma_r, \Sigma_\theta) = (\sigma_r, \sigma_\theta)/E$ are the non-dimensionalized stresses (with respect to the elastic modulus E), differentiation with respect to ξ is denoted by a superposed prime, ρ_0 is the reference density of the undeformed stress free state and the non-dimensionalized cavity expansion velocity

$$m = \frac{\dot{A}}{\sqrt{E/\rho_0}} \tag{4}$$

is the ratio between the cavity expansion velocity ($\dot{A}$) and the axial wave speed in a long elastic rod ($\sqrt{E/\rho_0}$).

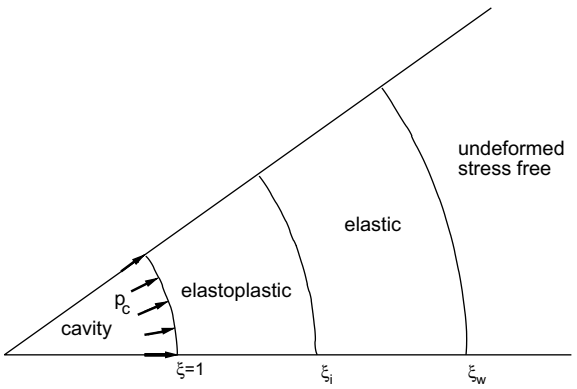

Fig. 1. Scheme of self similar field in dynamic expansion of a spherical cavity. Cavitation pressure is p_c. The radial coordinate ξ is non-dimensionalized with respect to the current radius of the cavity. The rigid/elastic wave front is at $\xi = \xi_w$. Plastic yielding occurs at the elastic/plastic interface $\xi = \xi_i$. The remote boundary at infinity is stress free.

Material response is modelled by the non-associated Drucker–Prager model (Durban and Fleck, 1997) which centers on the effective stress σ_e and plastic potential g defined by

$$\sigma_e = \tau + \mu\sigma_h \quad g = \tau + \eta\sigma_h, \tag{5}$$

where τ is the Mises effective stress, σ_h—the hydrostatic stress, and parameters (μ, η) reflect the plastic pressure sensitivity. Associated response is recovered when $\mu = \eta$ with a further reduction to the Mises solid for $\mu = \eta = 0$. The elastoplastic flow theory formulation follows from (5) in the hypoelastic form (Durban and Fleck, 1997),

$$\mathbf{D} = \left(\frac{1+v}{E}\right)\check{\boldsymbol{\sigma}} - \left(\frac{3v}{E}\right)\dot{\sigma}_h\mathbf{I} + \frac{\sigma_e\dot{\epsilon}_p}{g}\left(\frac{3\mathbf{S}}{2\tau} + \frac{\eta}{3}\mathbf{I}\right), \tag{6}$$

where $\mathbf{D}$ is the Eulerian strain rate, $\boldsymbol{\sigma}$—the Cauchy stress tensor, $\check{\boldsymbol{\sigma}}$—the Jaumann stress rate, $\mathbf{S}$—the stress deviator, $\mathbf{I}$—the second order unit tensor, v—Poisson's ratio and ϵ_p—the effective plastic strain and a known function of σ_e.

The derivation of (6) is based on the usual assumptions employed in constructing an elastoplastic flow theory; a normality rule for the plastic strain rate, the principle of plastic power equivalence, a Hookean elastic strain rate and linear decomposition of elastic and plastic strain rates. This constitutive equation can be used to model the material response of rock, concrete, soil and other porous solids. Experiments show that the rate of plastic volumetric strain in this kind of materials is below predictions of the associated model ($\mu = \eta$), and that was the motivation for constructing the non-associated model ($0 \leqslant \eta < \mu$). Non-associativity is defined by deviation from associativity through decreasing of η, which models a weaker material behavior (Durban and Fleck, 1997). Representative values of the parameter μ are $\mu = 1.311$ for castlegate sandstone and $\mu = 0.648$ for jurrasic shale.

For the spherical symmetric field induced by the cavity expansion, where $\tau = \sigma_\theta - \sigma_r$ and $\sigma_h = (\sigma_r + 2\sigma_\theta)/3$, we have from (5), with $\Sigma = \sigma_e/E$ and $G = g/E$, the non-dimensionalized versions of the effective stress and plastic potential

$$\Sigma = \Sigma_\theta - \Sigma_r + \tfrac{1}{3}\mu(\Sigma_r + 2\Sigma_\theta), \tag{7}$$

$$G = \Sigma_\theta - \Sigma_r + \tfrac{1}{3}\eta(\Sigma_r + 2\Sigma_\theta). \tag{8}$$

Likewise, the active components of the Eulerian strain rate become

$$\dot{\epsilon}_r = \frac{\mathrm{d}\dot{R}}{\mathrm{d}R} = \left(\frac{\dot{A}}{A}\right)\frac{\mathrm{d}V}{\mathrm{d}\xi} \quad \dot{\epsilon}_\theta = \dot{\epsilon}_\phi = \frac{\dot{R}}{R} = \left(\frac{\dot{A}}{A}\right)\frac{V}{\xi}. \tag{9}$$

Consequently, in the absence of material spin, the tensorial constitutive relation (6) separates into just two scalar relations, namely

$$V' = (V - \xi)\left[(\Sigma_r - 2v\Sigma_\theta)' - \left(1 - \frac{\eta}{3}\right)\left(\frac{\Sigma}{G}\right)\epsilon_p'\right], \tag{10}$$

$$\frac{V}{\xi} = (V - \xi)\left\{[-v\Sigma_r + (1-v)\Sigma_\theta]' + \left(\frac{1}{2} + \frac{\eta}{3}\right)\left(\frac{\Sigma}{G}\right)\epsilon_p'\right\}, \tag{11}$$

where we have used (2).

Finally, conservation of matter requires that

$$\frac{\dot{\rho}}{\rho} + \dot{\epsilon}_r + 2\dot{\epsilon}_\theta = 0 \tag{12}$$

or, on account of (9) and (2),

$$(V-\xi)\ln'\left(\frac{\rho}{\rho_0}\right)+V'+2\frac{V}{\xi}=0. \tag{13}$$

To sum up, we have four governing equations (3), (10), (11) and (13) with four unknowns $(\Sigma_r, \Sigma_\theta, V, \rho)$ whose dependence on ξ should be determined. Integration of that system is carried from the cavity's wall where

$$\xi = 1 : V = 1, \tag{14}$$

to the rigid/elastic interface (wave front) $\xi = \xi_w$ where we have $\rho = \rho_0$, as a stress free condition, and both velocity and stresses should vanish (Fig. 1) as will be verified in the next section.

In this formulation, the effective plastic strain ϵ_p is a given function of Σ, which describes the plastic strain-hardening (or softening). Plastic response is activated at the elastic/plastic interface $\xi = \xi_i$ where ϵ_p vanishes with $1 < \xi_i < \xi_w$ (Fig. 1). However, for elastic/perfectly plastic response ϵ_p is not known a priori and an extra algebraic equation is obtained from (7), in the post yield range,

$$\Sigma_\theta - \Sigma_r + \frac{1}{3}\mu(\Sigma_r + 2\Sigma_\theta) = \Sigma_y, \tag{15}$$

where Σ_y is the non-dimensional yield stress ($\Sigma_y = Y/E$ with Y denoting the yield stress). For that particular model, the elastic/plastic interface $\xi = \xi_i$ appears where Σ reaches the value of Σ_y.

3. The elastic zone

It is conceivable that at a distance from the cavity the deforming medium will respond in a purely elastic deformation with $\epsilon_p \equiv 0$. The constitutive equations (10) and (11) take then the simpler form, with no active plastic branch,

$$V' = (V-\xi)(\Sigma_r - 2v\Sigma_\theta)', \tag{16}$$

$$\frac{V}{\xi} = (V-\xi)[-v\Sigma_r + (1-v)\Sigma_\theta]', \tag{17}$$

which is now inserted in (13) to yield after integration the density relation

$$\frac{\rho}{\rho_0} = \exp[-(1-2v)(\Sigma_r + 2\Sigma_\theta)]. \tag{18}$$

Notice that the additional constant that appears upon integrating (13) has to vanish since ρ_0 is taken as the stress free value of ρ.

Subtracting (17) from (16) yields the integrable equation

$$\ln'\left(1-\frac{V}{\xi}\right) = -(1+v)(\Sigma_\theta - \Sigma_r)' \tag{19}$$

with the solution

$$V = \xi\{1 - \exp[-(1+v)(\Sigma_\theta - \Sigma_r)]\}, \tag{20}$$

accounting for the condition that V should vanish at the rigid/elastic interface $\xi = \xi_w$ where both stress components vanish alike. Substituting (20) back in (17) results in

$$-v\Sigma'_{\mathrm{r}} + (1-v)\Sigma'_{\theta} = \frac{1}{\xi}\left[1 - \mathrm{e}^{(1+v)(\Sigma_\theta - \Sigma_{\mathrm{r}})}\right]. \tag{21}$$

Likewise, we substitute (18) and (20) in the radial equation of motion (3) to obtain

$$\Sigma'_{\mathrm{r}} + \frac{2}{\xi}(\Sigma_{\mathrm{r}} - \Sigma_\theta) = m^2\xi^2(\Sigma'_{\mathrm{r}} - 2v\Sigma'_\theta)\mathrm{e}^{(1+4v)\Sigma_{\mathrm{r}} - (4-2v)\Sigma_\theta}. \tag{22}$$

The non-linear coupled system (21) and (22) can be further simplified since for elastic response of common solids both $|\Sigma_{\mathrm{r}}|$ and $|\Sigma_\theta|$ are extremely small by comparison with unity. Thus, we proceed with the linearized version

$$-v\Sigma'_{\mathrm{r}} + (1-v)\Sigma'_{\theta} = -\frac{1+v}{\xi}(\Sigma_\theta - \Sigma_{\mathrm{r}}), \tag{23}$$

$$\Sigma'_{\mathrm{r}} + \frac{2}{\xi}(\Sigma_{\mathrm{r}} - \Sigma_\theta) = m^2\xi^2(\Sigma'_{\mathrm{r}} - 2v\Sigma'_\theta). \tag{24}$$

The solution of Eqs. (23) and (24) is readily found in the form

$$\Sigma_{\mathrm{r}} = -\frac{2C}{3\xi^3} - \left(\frac{2vM^2}{1-2v}\right)\frac{C}{\xi} + B, \tag{25}$$

$$\Sigma_\theta = \frac{C}{3\xi^3} - \left(\frac{M^2}{1-2v}\right)\frac{C}{\xi} + B, \tag{26}$$

where (B, C) are integration constants, and

$$M^2 = \frac{(1+v)(1-2v)}{1-v}m^2 = \left(\frac{\dot{A}}{C_{\mathrm{E}}}\right)^2 \quad \text{with} \quad C_{\mathrm{E}} = \sqrt{\frac{(1-v)E}{(1+v)(1-2v)\rho_0}}. \tag{27}$$

Here, C_{E} denotes the linear elastic dilatation wave speed and M can be regarded as the cavity expansion Mach number. The radial material velocity is now obtained from (20), (25) and (26), as

$$V = \xi(1+v)(\Sigma_\theta - \Sigma_{\mathrm{r}}) = (1+v)\left(1 - M^2\xi^2\right)\frac{C}{\xi^2}, \tag{28}$$

again, under the assumption that $|\Sigma_{\mathrm{r}}|, |\Sigma_\theta| \ll 1$. The location of the wave front $\xi = \xi_{\mathrm{w}}$, where $V = 0$, as deduced from (28) is

$$\xi_{\mathrm{w}} = \frac{1}{M} = \frac{C_{\mathrm{E}}}{\dot{A}}, \tag{29}$$

implying a subsonic expansion field (where $M < 1$) which in turn defines, by (27), an upper limit on m. Combining (29) with (25) and (26) we find that the requirement that all stress components vanish at the rigid/elastic interface $\xi = \xi_{\mathrm{w}}$ gives

$$B = \frac{2(1+v)}{3(1-2v)}CM^3. \tag{30}$$

The remaining integration constant C will be determined upon imposing continuity conditions at the elastic/plastic interface $\xi = \xi_{\mathrm{i}}$. Since V should be positive we find from (28) that C must be positive as well. With the aid of (25), (26) and (30) the effective stress (7) is given, within the elastic zone, by

$$\Sigma = C\left(\frac{1}{\xi} - M\right)\left[\frac{1}{\xi^2} + \frac{M}{\xi} - \frac{2(1+\nu)}{3(1-2\nu)}\mu M^2\right]. \tag{31}$$

A simple algebraic analysis of (31) shows that Σ remains negative in a region bounded by the rigid/elastic interface (wave front) ξ_w and an inner radius ξ_0, where Σ vanishes, given by

$$\frac{1}{\xi_0} = \frac{M}{2}\left[\sqrt{1 + \frac{8(1+\nu)}{3(1-2\nu)}\mu} - 1\right], \tag{32}$$

under the condition

$$\mu > \frac{3(1-2\nu)}{1+\nu}. \tag{33}$$

This behavior of the effective stress reflects the plastic pressure sensitivity of the Drucker–Prager solid, in contrast with the Mises solid where the effective stress can never attain negative values. If (33) is violated then from (32) ξ_0 becomes non-physical ($\xi_0 \geqslant \xi_w$), so Σ remains positive within the entire elastic field and vanishes at the wave front. For hardening solids with no definite yield point (like the Ramberg–Osgood power law family) plastic strain is activated for any positive Σ. Thus, the existence of ξ_0 is important as the effective plastic strain is defined only for $\Sigma > 0$, so that initial yield is permissible only in the range of $\xi < \xi_0$. The elastic range, bounded by $\xi_0 \leqslant \xi \leqslant \xi_w$, is dominated by hydrostatic compression ($\sigma_h < 0$) which prevents the onset of plastic yield (5). Notice that under condition (33) ξ_0 is located between ξ_i and ξ_w for elastoplastic solids with a definite yield point, and marks the onset of plastic yielding for solids with no definite yield point.

4. The incompressible solid

With $\nu = \frac{1}{2}$ we find from (27) that $C_E \to \infty$ hence, by (29) $\xi_w \to \infty$ and the elastic zone extends to infinity.

For incompressible solids there are no density changes during deformation ($\rho \equiv \rho_0$) and the mass conservation equation (13) degenerates to a simple equation on V

$$V' + 2\frac{V}{\xi} = 0 \tag{34}$$

with the known solution (using the cavity wall condition $V(\xi = 1) = 1$)

$$V = \frac{1}{\xi^2}, \tag{35}$$

over the entire deformation range. Notice that the rate of volumetric strain for the Drucker–Prager model (6) is given by

$$\mathbf{I}\cdot\cdot\mathbf{D} = \frac{3(1-2\nu)}{E}\dot{\sigma_h} + \eta\frac{\sigma_e}{g}\dot{\epsilon_p}. \tag{36}$$

Thus, for an incompressible solid, which is plastic non-associated,

$$\nu = \frac{1}{2} \quad \text{and} \quad \eta = 0, \tag{37}$$

implying, by (35), that both constitutive equations (10) and (11) reduce to

$$\Sigma'_\theta - \Sigma'_{\mathrm{r}} + \frac{\Sigma}{G}\epsilon'_{\mathrm{p}} = \frac{2}{\xi - \xi^4}. \tag{38}$$

The radial equation of motion (3) is now

$$\Sigma'_{\mathrm{r}} + \frac{2}{\xi}(\Sigma_{\mathrm{r}} - \Sigma_\theta) = 2m^2\left(\frac{\xi^3 - 1}{\xi^5}\right), \tag{39}$$

forming together with (38) the governing equations for the two stress components (with Σ given by (7) and $G = \Sigma_\theta - \Sigma_{\mathrm{r}}$).

In the outer elastic field ($\xi_{\mathrm{i}} \leqslant \xi \leqslant \infty$) where $\epsilon_{\mathrm{p}} \equiv 0$ Eqs. (38) and (39) admit the solution

$$\Sigma_{\mathrm{r}} = -\frac{4}{3}\int_\xi^\infty \ln\left(\frac{x^3}{x^3 - 1}\right)\frac{\mathrm{d}x}{x} - 2m^2\left(\frac{1}{\xi} - \frac{1}{4\xi^4}\right), \tag{40}$$

$$\Sigma_\theta = \Sigma_{\mathrm{r}} + \frac{2}{3}\ln\left(\frac{\xi^3}{\xi^3 - 1}\right), \tag{41}$$

which is compatible with the stress free condition as $\xi \to \infty$.

Relations (40) and (41) represent the exact solution for elastic response of the incompressible hypoelastic solid. However, as ξ increases, the stresses in (40) and (41) approach asymptotically the values, for $\xi^3 \gg 1$,

$$\Sigma_{\mathrm{r}} = -\frac{4}{9\xi^3} - \frac{2m^2}{\xi}, \tag{42}$$

$$\Sigma_\theta = \frac{2}{9\xi^3} - \frac{2m^2}{\xi}. \tag{43}$$

This approximation coincides of course with the small strain linear elastic solution (25) and (26), at the limit of $\nu = \frac{1}{2}$, with B given by (30), when

$$C = \frac{2}{3}, \tag{44}$$

and the velocity profiles (28) and (35) become identical as well. Notice that, for the incompressible solid, the entire purely elastic field is in the small strains regime when $\xi_{\mathrm{i}}^3 \gg 1$. Also note that with $\nu = \frac{1}{2}$ we obtain from (32) that $\xi_0 = (\sqrt{3\mu}m)^{-1}$ (under the assumption of small strain elastic field). An exact equation for ξ_0 for the incompressible solid can be achieved from the exact elastic solution (40) and (41).

For elastic/perfectly plastic solids we have the yield condition, inside the plastic zone, expressed in (15). The solution of that equation along with (39) gives the plastic zone stresses ($1 \leqslant \xi \leqslant \xi_{\mathrm{i}}$)

$$\Sigma_{\mathrm{r}} = 2m^2\left[\frac{1}{\alpha - 1}\left(\frac{1}{\xi} - \frac{1}{\xi^\alpha}\right) - \frac{1}{\alpha - 4}\left(\frac{1}{\xi^4} - \frac{1}{\xi^\alpha}\right)\right] - \frac{P_{\mathrm{c}}}{\xi^\alpha} + \frac{\Sigma_{\mathrm{y}}}{\mu}\left(1 - \frac{1}{\xi^\alpha}\right), \tag{45}$$

$$\Sigma_\theta = \gamma_1\Sigma_{\mathrm{r}} + \gamma_2\Sigma_{\mathrm{y}}, \tag{46}$$

where $P_{\mathrm{c}} = -\Sigma_{\mathrm{r}}(\xi = 1)$ denotes the non-dimensionalized ($P_{\mathrm{c}} = p_{\mathrm{c}}/E$) cavitation pressure (Fig. 1) and

$$\alpha = \frac{2\mu}{1 + \frac{2}{3}\mu} \quad \gamma_1 = \frac{1 - \frac{1}{3}\mu}{1 + \frac{2}{3}\mu} \quad \gamma_2 = \frac{1}{1 + \frac{2}{3}\mu}. \tag{47}$$

Continuity of radial stress and plastic yield (15) at the elastic/plastic interface ($\xi = \xi_{\mathrm{i}}$) requires that the elastic stresses (40) and (41) are equal to the plastic stresses (45) and (46) at the interface. By that we obtain two exact equations, with ξ_{i} and P_{c} as unknowns,

$$\ln\left(\frac{\xi_i^3-1}{\xi_i^3}\right)+\alpha\int_{\xi_i}^{\infty}\ln\left(\frac{\xi^3}{\xi^3-1}\right)\frac{d\xi}{\xi}+\frac{3}{2}\alpha m^2\left(\frac{1}{\xi_i}-\frac{1}{4\xi_i^4}\right)+\frac{3}{2}\gamma_2\Sigma_y=0, \tag{48}$$

$$P_c=2m^2\left[\left(\frac{1}{4-\alpha}\right)\xi_i^{\alpha-4}+\left(\frac{1}{1-\alpha}\right)\left(\frac{3}{4-\alpha}-\xi_i^{\alpha-1}\right)\right]-\frac{\Sigma_y}{\mu}+\frac{4}{3\alpha}\xi_i^{\alpha}\ln\left(\frac{\xi_i^3}{\xi_i^3-1}\right). \tag{49}$$

The value of ξ_i is determined from (48) by a standard numerical procedure and the corresponding cavitation pressure follows at once from (49). Sample numerical solutions for the stress profiles are illustrated in Fig. 2 for $m=0.25$ and with several values of μ. The cavitation pressure appears to increase with μ while ξ_i decreases with μ.

If μm^2 is not too large we may assume that $\xi_i^3\gg 1$ and replace (40) and (41) by the approximations (42) and (43). Substituting (42) and (43) in (46) we arrive, for $\xi=\xi_i$, at a cubic equation for the elastic/plastic interface location, namely

$$\frac{1}{\xi_i^3}-\frac{3\mu m^2}{\xi_i}-\frac{3}{2}\Sigma_y=0. \tag{50}$$

Once the physical root of this equation has been located, the cavitation pressure P_c follows, upon equating (42) with (45) at $\xi=\xi_i$ and using (50) or simply by applying $\xi_i^3\gg 1$ to (49), in the form

$$P_c=\frac{4}{3\alpha}\xi_i^{\alpha-3}+\frac{2m^2}{1-\alpha}\left(\frac{3}{4-\alpha}-\xi_i^{\alpha-1}\right)-\frac{\Sigma_y}{\mu}. \tag{51}$$

A useful approximation of ξ_i can be extracted from (50) by expanding the root in powers of μm^2, resulting in the leading terms

$$\frac{1}{\xi_i}=\left(\frac{3}{2}\Sigma_y\right)^{1/3}+\mu m^2\left(\frac{3}{2}\Sigma_y\right)^{-1/3}+\cdots \tag{52}$$

and this approximation is valid for $3\mu m^2\ll\left(\frac{3}{2}\Sigma_y\right)^{2/3}$. However, an alternative expansion of ξ_i, in ascending powers of Σ_y, can be written as

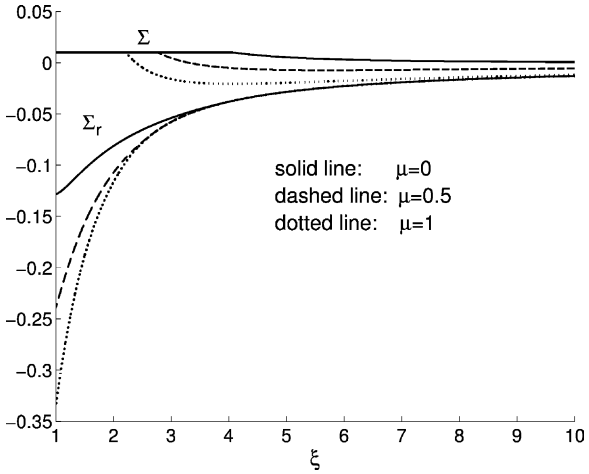

Fig. 2. Radial stress (Σ_r) and effective stress (Σ) profiles at different levels of pressure sensitivity μ. Results are for an incompressible solid ($\nu=\frac{1}{2},\eta=0$) with elastic/perfectly plastic response ($\Sigma_y=0.01$). Expansion velocity is $m=0.25$.

$$\frac{1}{\xi_{\mathrm{i}}} = \left(3\mu m^2\right)^{1/2} + \frac{\Sigma_{\mathrm{y}}}{4\mu m^2} + \cdots, \tag{53}$$

which is valid for $3\mu m^2 \gg \left(\frac{3}{2}\Sigma_{\mathrm{y}}\right)^{2/3}$ provided that μm^2 is not too large. Notice that the first term in (53) is exactly ξ_0^{-1}.

In the absence of pressure sensitivity ($\mu = 0$) we recover from (52) the known approximated result (Hill, 1950) $\xi_{\mathrm{i}} = \left(\frac{2}{3\Sigma_{\mathrm{y}}}\right)^{1/3}$ along with the classical approximate cavitation pressure (Hopkins, 1960), from (51),

$$P_{\mathrm{c}} = \frac{2}{3}\Sigma_{\mathrm{y}} \ln\left(\frac{2}{3\Sigma_{\mathrm{y}}}\right) + \frac{2}{3}\Sigma_{\mathrm{y}} + \frac{3}{2}m^2. \tag{54}$$

In the same spirit it is possible to obtain approximate solutions of (49), with the aid of (50)–(53), at different levels of accuracy. Using (50) we can rewrite (51) in the equivalent form

$$P_{\mathrm{c}} = \frac{\Sigma_{\mathrm{y}}}{\mu}\left(\xi_{\mathrm{i}}^{\alpha} - 1\right) + \frac{2m^2}{1-\alpha}\left(\frac{3}{4-\alpha} - \alpha\xi_{\mathrm{i}}^{\alpha-1}\right) + \frac{2\alpha\xi_{\mathrm{i}}^{\alpha-3}}{3\mu(3-\alpha)} \tag{55}$$

and a further substitution of the first order approximations (52) and (53) results in the useful expressions

$$P_{\mathrm{c}} = \frac{\Sigma_{\mathrm{y}}}{\mu}\left[\left(\frac{2}{3\Sigma_{\mathrm{y}}}\right)^{\frac{\alpha}{3}} - 1\right] + \frac{2m^2}{1-\alpha}\left[\frac{3}{4-\alpha} - \alpha\left(\frac{2}{3\Sigma_{\mathrm{y}}}\right)^{\frac{\alpha-1}{3}}\right] + \frac{2\alpha}{3\mu(3-\alpha)}\left(\frac{2}{3\Sigma_{\mathrm{y}}}\right)^{\frac{\alpha}{3}-1} \tag{56}$$

for $3\mu m^2 \ll \left(\frac{3}{2}\Sigma_{\mathrm{y}}\right)^{2/3} \ll 1$, and

$$P_{\mathrm{c}} = \frac{\Sigma_{\mathrm{y}}}{\mu}\left[\left(\sqrt{3\mu}m\right)^{-\alpha} - 1\right] + \frac{2m^2}{1-\alpha}\left[\frac{3}{4-\alpha} - \alpha\left(\sqrt{3\mu}m\right)^{1-\alpha}\right] + \frac{2\alpha}{3\mu(3-\alpha)}\left(\sqrt{3\mu}m\right)^{3-\alpha} \tag{57}$$

for $\left(\frac{3}{2}\Sigma_{\mathrm{y}}\right)^{2/3} \ll 3\mu m^2 \ll 1$.

These relations reveal the influence of pressure sensitivity and non-associativity since plastic incompressibility ($\eta = 0$) is here also an extreme case of non-associativity.

Fig. 3 displays the dependence of the cavitation pressure P_{c} on expansion velocity m and pressure sensitivity μ. Both parameters cause an increase in P_{c}, as they become larger, with a parabolic like influence of m, but notice that only (56) has an exact parabolic influence of material inertia. The curves in Fig. 3 have

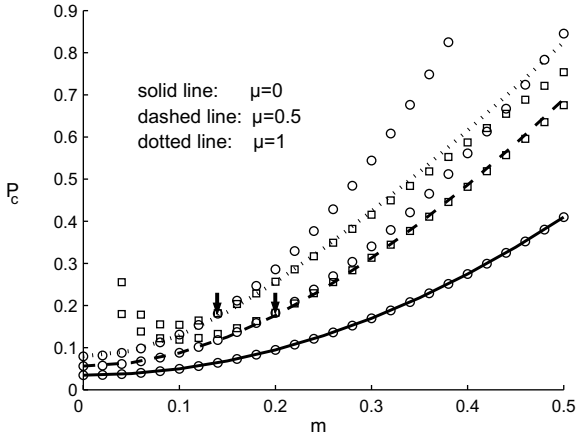

Fig. 3. Variation of cavitation pressure P_{c} with expansion velocity m for a few values of μ. Results are for an incompressible solid ($\nu = \frac{1}{2}, \eta = 0$) with elastic/perfectly plastic response ($\Sigma_{\mathrm{y}} = 0.01$).

been evaluated numerically from the exact relations (48) and (49) while circle markers represent the approximation (56), and square markers represent the approximation (57). The top–down arrows indicate the locations $(m^* = (\frac{1}{3\mu})^{\frac{1}{2}}(\frac{3\Sigma_Y}{2})^{\frac{1}{3}})$ where the two approximations (56) and (57) coincide.

For hardening incompressible solids we use the definition of the effective stress in (7) to eliminate Σ_θ from the governing equations (38) and (39). This leads to a system of two equations for Σ_r and Σ, namely

$$\gamma_2(\Sigma' - \mu\Sigma_r') + \frac{1}{\gamma_2}\left(\frac{\Sigma\Sigma'\frac{d\epsilon_p}{d\Sigma}}{\Sigma - \mu\Sigma_r}\right) = \frac{2}{\xi - \xi^4}, \tag{58}$$

$$\Sigma_r' - \frac{2\gamma_2}{\xi}(\Sigma - \mu\Sigma_r) = 2m^2\left(\frac{\xi^3 - 1}{\xi^5}\right), \tag{59}$$

where γ_2 is defined in (47). These equations can be solved numerically over the plastic range $1 \leqslant \xi \leqslant \xi_i$ for any hardening characteristic ϵ_p. The elastic/plastic interface location $\xi = \xi_i$ can be found using the elastic solution (40) and (41) under the boundary condition

$$\xi = \xi_i : \epsilon_p = 0, \tag{60}$$

which can be translated to a specific condition on Σ depending on the hardening law. Furthermore, at the elastic/plastic interface $\xi = \xi_i$ the stresses should comply with the elastic solution (40) and (41). Figs. 4 and 5 display the stresses and cavitation pressure for a power-hardening solid $(\epsilon_p = 100\Sigma^2)$ of the Ramberg–Osgood type. These figures have been evaluated numerically from (58) and (59).

For the Mises solid $(\mu = 0, \gamma_2 = 1)$ Eq. (58) admits an exact solution for any hardening characteristic,

$$\epsilon = \frac{2}{3}\ln\left(\frac{\xi^3}{\xi^3 - 1}\right) + \epsilon_*, \tag{61}$$

where $\epsilon = \Sigma + \epsilon_p$ is the total strain and ϵ_* is an integration constant. In fact, this solution also covers the elastic zone where $\epsilon_p \equiv 0$, so by (41) we have to take $\epsilon_* = 0$. Notice that for the incompressible Mises solid the total strain does not depend on m. The radial stress follows from (59) as

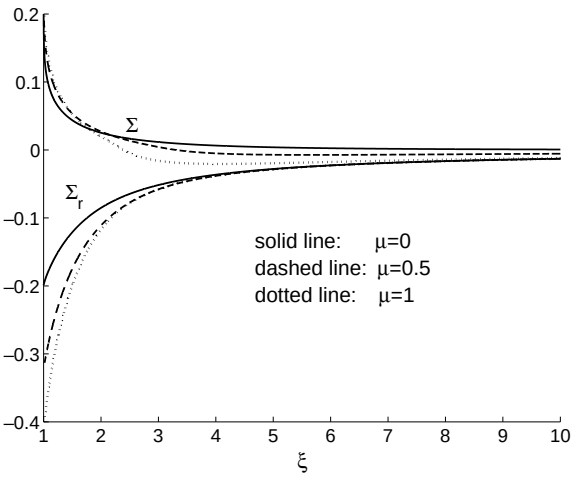

Fig. 4. Radial stress (Σ_r) and effective stress (Σ) profiles for an incompressible ($\nu = \frac{1}{2}, \eta = 0$) power-hardening ($\epsilon_p = 100\Sigma^2$) solid. Expansion velocity is $m = 0.25$ and values of μ are shown in the figure.

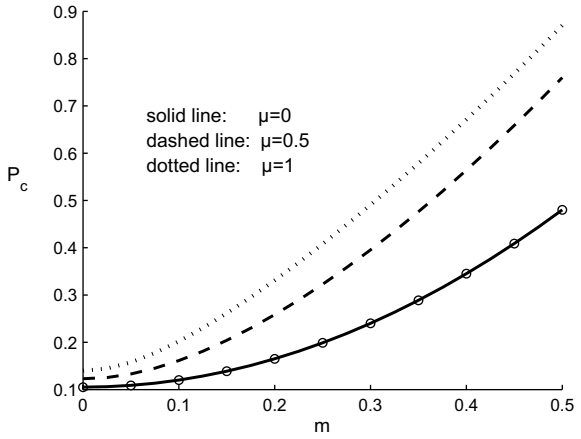

Fig. 5. Variation of cavitation pressure P_c with expansion velocity m for an incompressible material ($\nu = \frac{1}{2}, \eta = 0$) with a power law characteristic ($\epsilon_p = 100\Sigma^2$). Values of pressure sensitivity parameter are indicated in the figure. Circle markers show the exact Mises results from (64).

$$\Sigma_r = -2\int_{\xi}^{\infty} \Sigma(x)\frac{dx}{x} - 2m^2\left(\frac{1}{\xi} - \frac{1}{4\xi^4}\right), \tag{62}$$

where $\Sigma(\xi)$ is given implicitly in (61) and $\epsilon_* = 0$. Thus, the cavitation pressure is simply

$$P_c = 2\int_{1}^{\infty} \Sigma(\xi)\frac{d\xi}{\xi} + \frac{3}{2}m^2. \tag{63}$$

This can be rewritten with the effective Mises stress as the independent variable in the form

$$P_c = \int_{0}^{\infty} \frac{\Sigma d\epsilon}{e^{\frac{3}{2}\epsilon} - 1} + \frac{3}{2}m^2. \tag{64}$$

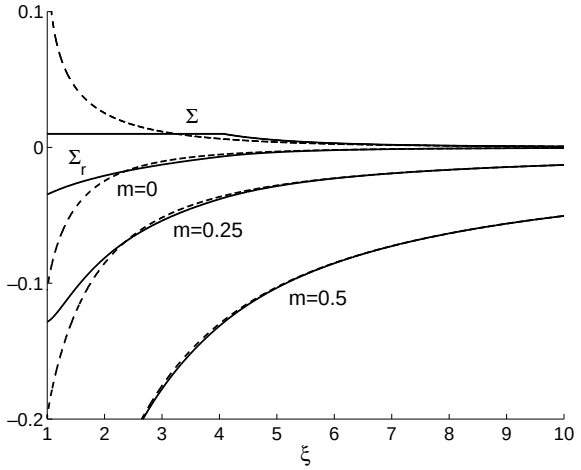

Fig. 6. Radial stress (Σ_r) and effective stress (Σ) profiles for an incompressible Mises solid ($\mu = \eta = 0, \nu = \frac{1}{2}$). Results are for elastic/perfectly plastic response $\Sigma_y = 0.01$ (solid line) and for power-hardening law with $\epsilon_p = 100\Sigma^2$ (dashed line). Values of expansion velocity are indicated on curves, but effective stress profile is independent of m.

The integral, evaluated for any hardening characteristic $\epsilon(\Sigma)$, is a purely constitutive parameter. As it stands, relation (64) is accurate and can be evaluated for any hardening or softening response where the dependence of ϵ on Σ is known, including the special case of the elastic/perfectly plastic solid. Fig. 5 displays an illustration for this accurate relation (designated by circle markers). Fig. 6 shows a few representative curves for stress profiles in an incompressible Mises solid with perfectly plastic ($\Sigma_y = 0.01$), and power-hardening response given by $\epsilon_p = 100\Sigma^2$.

5. The solid with the associated flow rule

The associated Drucker–Prager model is obtained when $\mu = \eta$, implying that the plastic potential G is identical with the effective stress (7) and (8). The constitutive equations (10) and (11) are now given by the simpler version

$$V' = (V - \xi)\left[\Sigma_r - 2v\Sigma_\theta - \left(1 - \frac{\mu}{3}\right)\epsilon_p\right]', \tag{65}$$

$$\frac{V}{\xi} = (V - \xi)\left[- v\Sigma_r + (1 - v)\Sigma_\theta + \left(\frac{1}{2} + \frac{\mu}{3}\right)\epsilon_p\right]'. \tag{66}$$

Inserting (65) and (66) in (13) and integrating over ξ we get

$$\rho = \rho_0 e^{-\Theta} \quad \text{with} \quad \Theta = (1 - 2v)(\Sigma_r + 2\Sigma_\theta) + \mu\epsilon_p, \tag{67}$$

where again, as in (18), ρ_0 is the stress free reference density.

Next, we subtract (66) from (65) and integrate the equation thus obtained. This gives

$$V = \xi\left(1 - e^{-\Phi}\right) \quad \text{with} \quad \Phi = (1 + v)(\Sigma_\theta - \Sigma_r) + \frac{3}{2}\epsilon_p, \tag{68}$$

where the condition that V should vanish at the wave front has been used. Substituting the velocity (68) back in (66) gives

$$\left[- v\Sigma_r + (1 - v)\Sigma_\theta + \left(\frac{1}{2} + \frac{\mu}{3}\right)\epsilon_p\right]' = \frac{1}{\xi}\left(1 - e^{\Phi}\right). \tag{69}$$

Similarly, with the aid of (67) and (68), the equation of motion (3) becomes

$$\Sigma_r' + \frac{2}{\xi}(\Sigma_r - \Sigma_\theta) = m^2\xi^2\left[\Sigma_r - 2v\Sigma_\theta - \left(1 - \frac{\mu}{3}\right)\epsilon_p\right]' e^{-\Theta - 2\Phi}. \tag{70}$$

A further simplification of (69) and (70) is possible upon elimination of Σ_θ with the aid of the effective stress relation (7). By that we obtain two equations for Σ_r and Σ that can be solved by available numerical methods. As an example, we have studied (Fig. 7) the effect of pressure sensitivity μ on the cavitation pressure, in the absence of elastic compressibility ($v = \frac{1}{2}$). The coupled effect of m and μ appears to be quite appreciable in increasing the value of P_c. The circle markers in Fig. 7 represent the exact solution (64) for the incompressible Mises solid. Another illustration to the influence of pressure sensitivity is shown in Fig. 8 which displays the variation of the quasi-static ($m = 0$) cavitation pressure with the elastic-compressibility parameter $\beta = 1–2v$. The circle markers in Fig. 8 represent the exact solution of P_c for the quasi-static, elastic compressible Mises solid obtained by Durban and Baruch (1976). Curves of cavitation pressure in an elastic compressible ($v = \frac{1}{3}$) associated solid are displayed in Fig. 9, as evaluated from Eqs. (69) and (70). By

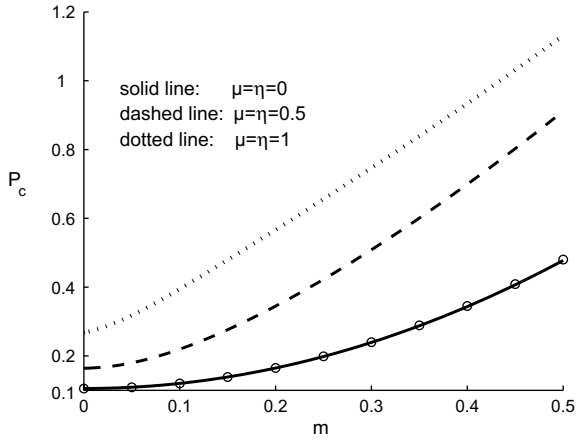

Fig. 7. Variation of cavitation pressure P_c with expansion velocity m for an elastic incompressible ($v = \frac{1}{2}$) associated solid. Power-hardening law with $\epsilon_p = 100\Sigma^2$. Circle markers show the exact Mises results from (64).

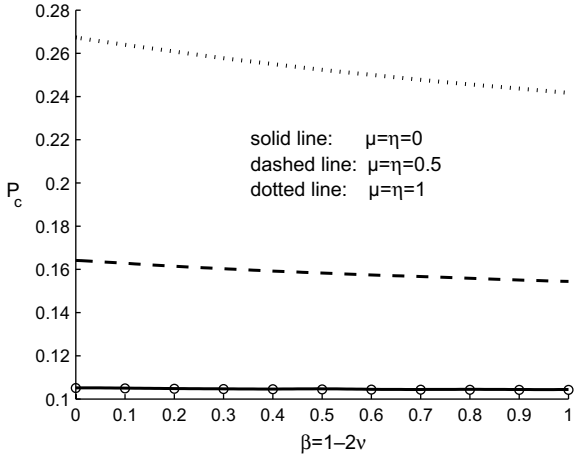

Fig. 8. Variation of cavitation pressure P_c for quasi-static ($m = 0$) expansion in an elastic compressible ($\beta = 1 - 2v$) associated solid. Power-hardening law with $\epsilon_p = 100\Sigma^2$. Circle markers show the exact Mises solution (Durban and Baruch, 1976).

comparison, at small values of m, plastic compressibility has a much stronger influence on P_c which is hardly sensitive to changes in v.

For associated elastic/perfectly plastic solids the effective plastic strain becomes an unknown variable but we have the extra algebraic equation for the yield condition (15). Here we do not elaborate on this particular case, but mention briefly that ϵ_p is easily eliminated between the constitutive relations (65) and (66). Also, from (67) and (68) we can write, for the plastic range,

$$\frac{\rho}{\rho_0} = \left(1 - \frac{V}{\xi}\right)^{-\frac{2}{3}\mu} \exp\left[-(1-2v)(\Sigma_r + 2\Sigma_\theta) - \frac{2}{3}\mu(1+v)(\Sigma_\theta - \Sigma_r)\right], \tag{71}$$

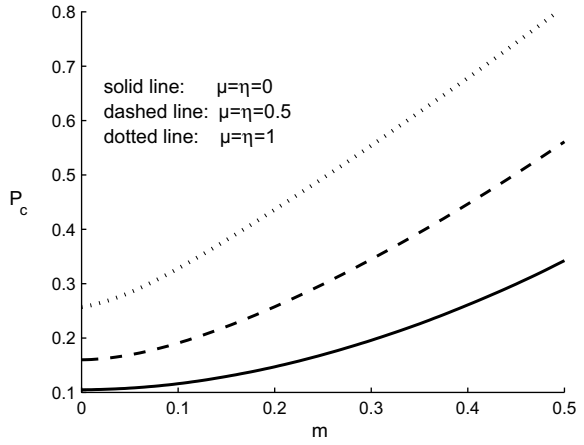

Fig. 9. Effect of pressure sensitivity and expansion velocity on cavitation pressure in an elastic compressible ($\nu = \frac{1}{3}$) associated solid. Power-hardening law with $\epsilon_{\mathrm{p}} = 100\Sigma^2$.

which does not contain ϵ_{p}. Substituting the density ratio (71) in the equation of motion (3) produces a third equation for the unknowns $(\Sigma_{\mathrm{r}}, \Sigma_\theta, V)$. A further reduction to a system of two equations with two unknowns (Σ_{r}, V) is straightforward.

6. Asymptotic analysis of the near cavity boundary layer

The behavior of the thin layer adjacent to cavity wall ($\xi = 1$) is dominated by the plastic branch of the constitutive relations (10) and (11), so asymptotically (as $\xi \to 1$) $\epsilon \to \epsilon_{\mathrm{p}}$, and we obtain the near wall relations for solids with an associated flow rule

$$V' = -\left(1 - \frac{\mu}{3}\right)(V - \xi)\epsilon'_{\mathrm{p}} \qquad \frac{V}{\xi} = \left(\frac{1}{2} + \frac{\mu}{3}\right)(V - \xi)\epsilon'_{\mathrm{p}}. \tag{72}$$

These relations can be combined to produce the differential relation

$$\frac{\mathrm{d}V}{V} = -2\gamma_1 \frac{\mathrm{d}\xi}{\xi} \tag{73}$$

or, recalling that $V(\xi = 1) = 1$,

$$V = \xi^{-2\gamma_1}. \tag{74}$$

Introducing now the plastic boundary layer coordinate $\delta = \xi - 1$, with $\delta \ll 1$, we find from (74) the boundary layer velocity profile

$$V \sim 1 - 2\gamma_1\delta. \tag{75}$$

Relations (74) and (75) are valid also for a solid with a non-associated flow rule ($G \neq \Sigma$) but with η replacing μ in expression (47) for γ_1.

Inserting (75) in the second of (72) and integrating we find the asymptotic behavior of the effective plastic strain, for the solid with an associated flow rule,

$$\epsilon_{\mathrm{p}} \sim \frac{2}{3} \ln\left(\frac{1}{\delta}\right), \tag{76}$$

indicating, as expected, extremely high levels of strain near the cavity. It is interesting to note that the leading term (76) is independent of material properties. In Section 7, the curves in Fig. 11 detailing ϵ_{p} near the wall, corroborate expansion (76) by showing little sensitivity to variations in μ and η. The analogous expansion for the effective stress can be deduced from (76) since ϵ_{p} depends on Σ. With the power law $\epsilon_{\mathrm{p}} = K\Sigma^n$, for example, we find

$$\Sigma \sim \left[\frac{2}{3K} \ln\left(\frac{1}{\delta}\right)\right]^{\frac{1}{n}}, \tag{77}$$

where (K, n) are material parameters. It can be seen that strain-hardening raises effective stress gradients within the boundary layer. In Section 4, the curves in Fig. 4 detailing Σ near the wall, corroborate expansion (77) by showing little sensitivity to variations in μ.

The density is given in (67) and upon neglect of elastic terms (valid only for $\mu > 0$), it becomes, within the cavity boundary layer, for the solid with an associated flow rule,

$$\rho \sim \rho_0 \mathrm{e}^{-\mu\epsilon_{\mathrm{p}}} \sim \rho_0 \delta^{\frac{2}{3}\mu} \tag{78}$$

with the aid of (76).

The asymptotic behavior of the radial stress is obtained from the equation of motion (3) in its asymptotic version, with the aid of (74) and (78),

$$\Sigma_{\mathrm{r}}' + \frac{2}{\xi}(\Sigma_{\mathrm{r}} - \Sigma_\theta) = 2m^2\gamma_1\left(\xi^{-2\gamma_1} - \xi^{-1-4\gamma_1}\right)\mathrm{e}^{-\mu\epsilon_{\mathrm{p}}} \tag{79}$$

with ϵ_{p} given by (76). Furthermore, the circumferential stress in (79) can be eliminated through the effective stress relation (7), resulting in a single equation for the radial stress, namely

$$\Sigma_{\mathrm{r}}' + \alpha\frac{\Sigma_{\mathrm{r}}}{\xi} = 2\gamma_2\frac{\Sigma}{\xi} + 2m^2\gamma_1\left(\xi^{-2\gamma_1} - \xi^{-1-4\gamma_1}\right)\mathrm{e}^{-\mu\epsilon_{\mathrm{p}}}. \tag{80}$$

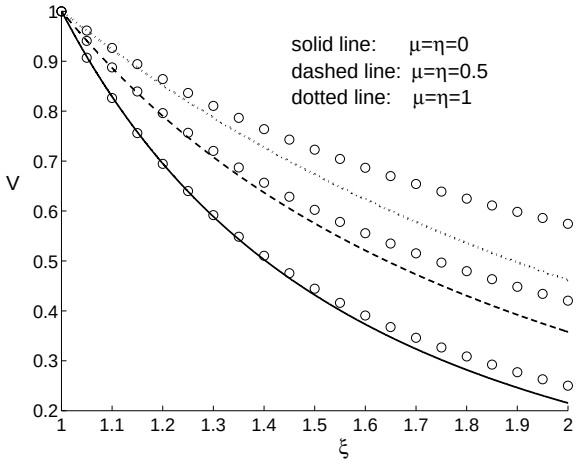

Fig. 10. Velocity profiles within near cavity boundary layer. Power-hardening material ($\epsilon_{\mathrm{p}} = 100\Sigma^2$) with $m = 0.25$ and $v = \frac{1}{3}$. The asymptotic expression (74) is indicated by circle markers.

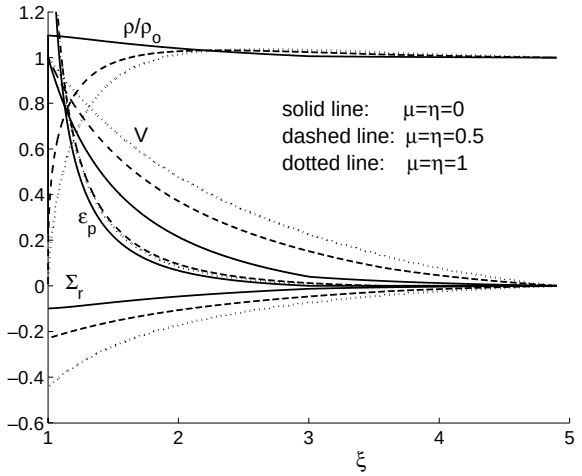

Fig. 11. Radial profiles of essential field variables for an elastic compressible ($\nu = \frac{1}{3}$) perfectly plastic ($\Sigma_y = 0.01$) associated solid. Results are for $m = 0.25$ and with several values of pressure sensitivity.

With Σ regarded as a known function of ϵ_p, given by (76), it is possible to evaluate the asymptotic behavior of Σ_r by direct integration of (80), employing the condition $\Sigma_r(\xi = 1) = -P_c$. A particularly simple example is furnished by the perfectly plastic model where $\Sigma = \Sigma_y$ and (80) gives the asymptotic profile

$$\Sigma_r \sim -P_c + 2\gamma_2(\Sigma_y + \mu P_c)\delta + m^2\gamma_1\gamma_2(1 + 2\gamma_1)\delta^{2+\frac{2}{3}\mu}, \tag{81}$$

where we have retained only the leading dynamic term.

The asymptotic expression (74) is compared in Fig. 10 with accurate numerical calculations for the velocity profile in the near cavity boundary layer. It appears that the validity of (74) decreases with pressure sensitivity, but remains in good agreement with numerical data near the wall.

7. Concluding remarks

We have presented a detailed analysis of steady-state self-similar expansion of a pressurized spherical cavity in a pressure sensitive elastoplastic infinite medium. The study covers a wide range of material parameters pertaining to the Drucker–Prager plasticity model.

Radial dependence of essential field variables (radial stress Σ_r, effective plastic strain ϵ_p, radial velocity V, density ratio ρ/ρ_0) are shown in Fig. 11 for an elastic compressible, perfectly plastic solid with an associated flow rule. A similar chart is displayed in Fig. 12 for an elastic compressible, power-hardening solid with an associated flow rule. Both figures are for representative material properties and have been evaluated numerically from the exact relations derived in this study.

The common observation that can be deduced from Figs. 11 and 12 is that pressure sensitivity increases the value of $|\Sigma_r|$ (and hence also the cavitation pressure). Similarly, the radial material velocity increases with pressure sensitivity. Both the effective plastic strain in Fig. 11, and the effective stress in Fig. 12 are not much influenced by pressure sensitivity. Variations in density ratio are confined to a narrow zone near the cavity and show higher boundary layer gradients as pressure sensitivity decreases.

Another important observation related to non-associativity can be deduced upon comparing Fig. 5 with Fig. 7. It can be seen that non-associativity (deviation from associativity ($\mu = \eta$) through decreasing of η) induces a weaker material behavior, as expected. The influence of plastic compressibility (η) can also be

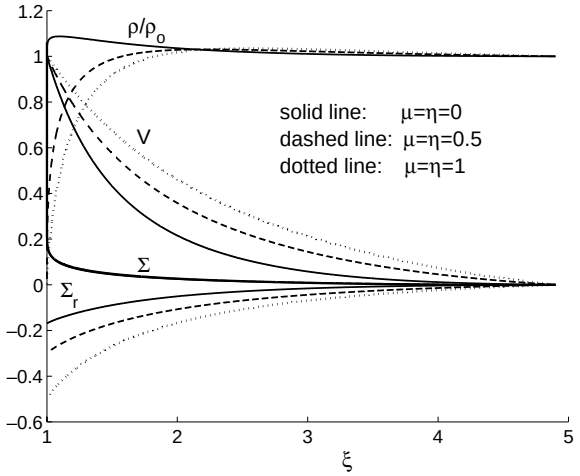

Fig. 12. Radial profiles of essential field variables for an elastic compressible ($\nu = \frac{1}{3}$) power-hardening ($\epsilon_p = 100\Sigma^2$) associated solid. Results are for $m = 0.25$ and with several values of pressure sensitivity. Variations in Σ are too small to be observed.

deduced upon comparing Figs. 5 and 7. It can be seen that while the cavitation pressure decreases when elastic compressibility ($\beta = 1–2\nu$) increases (Fig. 8 and comparison between Figs. 7 and 9) the cavitation pressure increases when plastic compressibility increases (comparison between Figs. 5 and 7). It is clear that the strongest material is the associated elastically incompressible material (Fig. 7), so the fully incompressible material discussed in Section 4, which is extremely non-associated, is weaker (Fig. 5).

The blend of analytical, numerical and asymptotic results derived in this study, along with some useful approximate relations, provides a sound basis for the understanding of dynamic cavity expansion phenomena in pressure sensitive elastoplastic media. The body of data exposed here is a natural generalization of the classical analysis (Hopkins, 1960) for the standard Mises solid. Application to penetration models allows to account quite accurately for both media porosity and strain-hardening, apart from the influence of non-associativity. In fact, it should not be difficult to incorporate in the analysis the behavior of media which exhibits plastic strain softening.

Acknowledgements

One of us (D.D) wishes to acknowledge the support of the Sydney Goldstein Chair in Aerospace Engineering. Part of this study was supported by the fund for the promotion of research at the Technion.

References

Durban, D., Baruch, M., 1976. On the problem of a spherical cavity in an infinite elasto-plastic medium. J. Appl. Mech. 43, 633–638.

Durban, D., Fleck, N.A., 1997. Spherical cavity expansion in a Drucker–Prager solid. J. Appl. Mech. 64, 743–750.

Forrestal, M.J., Luk, V.K., 1988. Dynamic spherical cavity-expansion in a compressible elastic–plastic solid. J. Appl. Mech. 55, 275–279.

Forrestal, M.J., Tzou, D.Y., 1997. A spherical cavity expansion penetration model for concrete targets. Int. J. Solids Struct. 34, 4127–4146.

Hill, R., 1950. The Mathematical Theory of Plasticity. Oxford University Press, London.

Hopkins, H.G., 1960. Dynamic expansion of spherical cavities in metal. In: Sneddon, I.N., Hill, R. (Eds.), Progress in Solid Mechanics, vol. 1. North-Holland, Amsterdam.

Luk, V.K., Forrestal, M.J., Amos, D.E., 1991. Dynamic spherical cavity expansion of strain-hardening materials. J. Appl. Mech. 58, 1–6.

Macek, R.W., Duffey, T.A., 2000. Finite cavity expansion method for near-surface effects and layering during earth penetration. Int. J. Impact Engng. 24, 239–258.

Masri, R., 2001. Dynamic spherical cavitation in a porous elastoplastic medium. M.Sc. research thesis, Technion, Haifa, Israel (In Hebrew).

Satapathy, S., 2001. Dynamic spherical cavity expansion in brittle ceramics. Int. J. Solids Struct. 38, 5833–5845.